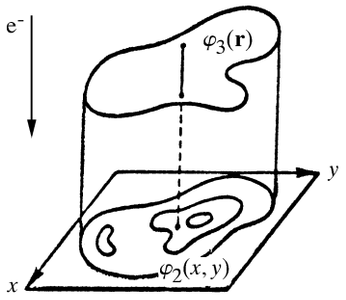

Fig. 2.5.6.1. A three-dimensional object φ_3 and its two-dimensional projection φ_2. The electron beam penetrates the specimen in the direction of the z axis.

The projection direction is defined by a unit vector $\boldsymbol{\tau}(\theta, \psi)$ and it is formed on the plane $\mathbf{x}$ perpendicular to $\boldsymbol{\tau}$. The set of various projections $\varphi_2(\mathbf{x}_{\tau_i}) = \varphi_{2_i}(\mathbf{x}_i)$ may be assigned by a discrete or continuous set of points on a unit sphere $|\tau| = 1$ (Fig. 2.5.6.2).

In Fourier space, the relation between an object and its projection is referred to as the central section theorem: the Fourier transformation of projection φ_2 of a 3D object φ_3 is the central (*i.e.*, passing though the origin of reciprocal space) 2D plane cross section of a 3D transform perpendicular to the projection vector (Bracewell, 1956; DeRosier & Klug, 1968; Crowther, Amos *et al.*, 1970). In Cartesian coordinates, a 3D Fourier transform is

$$\begin{aligned}\mathscr{F}[\varphi_3(\mathbf{r})] &= \Phi_3(u, v, w) \\ &= \iiint \varphi_3(x, y, z) \exp\{2\pi i(ux + vy + wz)\}\, \mathrm{d}x\, \mathrm{d}y\, \mathrm{d}z.\end{aligned} \tag{2.5.6.6}$$

The transform of projection $\varphi_2(x, y)$ along z is

$$\begin{aligned}\mathscr{F}[\varphi_2(x, y)] &= \Phi_3(u, v, 0) \\ &= \iiint \varphi_3(x, y, z) \exp\{2\pi i(ux + vy + 0z)\}\, \mathrm{d}x\, \mathrm{d}y\, \mathrm{d}z \\ &= \iiint \varphi_3(x, y, z)\, \mathrm{d}z \exp\{2\pi i(ux + vy)\}\, \mathrm{d}x\, \mathrm{d}y \\ &= \iint \varphi_2(x, y) \exp\{2\pi i(ux + vy)\}\, \mathrm{d}x\, \mathrm{d}y \\ &= \Phi_2(u, v).\end{aligned} \tag{2.5.6.7}$$

In the general case of projecting along the vector $\boldsymbol{\tau}$, the central section theorem is

$$\mathscr{F}[\varphi_2(\mathbf{x}_\tau)] = \Phi_3(\mathbf{u}_\tau), \quad \mathbf{u}_\tau \perp \boldsymbol{\tau}. \tag{2.5.6.8}$$

From this theorem it follows that the inversion of the 3D ray transform is possible if there is a continuous set of projections φ_τ corresponding to the motion of the vector $\boldsymbol{\tau}(\theta, \psi)$ over any continuous line connecting the opposite points on the unit sphere (Fig. 2.5.6.2) (Orlov's condition: Orlov, 1976). This result is evidenced by the fact that in this case the cross sections $\mathscr{F}[\varphi_2(\mathbf{x}_\tau)]$ that are perpendicular to $\boldsymbol{\tau}$ in Fourier space continuously cover the whole Fourier space, *i.e.*, they yield $\mathscr{F}[\varphi_3(\mathbf{r})]$ and thereby determine $\varphi_3(\mathbf{r}) = \mathscr{F}^{-1}[\Phi_3(\mathbf{u})]$.

In single-particle reconstruction, imaged objects are randomly and nonuniformly oriented on the substrate at different angles (Frank, 2006) and the distribution of their orientations is beyond our control; therefore, the practical impact of Orlov's condition is limited. In fact, it is more useful to determine *a posteriori*, *i.e.*, after the 3D reconstruction of the macromolecule is computed, how well the Fourier space was covered. This can be done by calculating the distribution of the 3D spectral signal-to-noise ratio (Penczek, 2002).

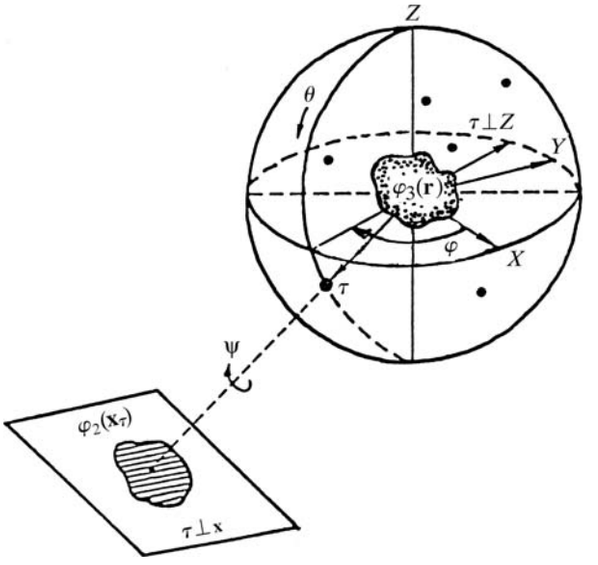

Fig. 2.5.6.2. The projection sphere and projection $\varphi_2(\mathbf{x}_\tau)$ of $\varphi_3(\mathbf{r})$ along $\boldsymbol{\tau}$ onto the plane $\boldsymbol{\tau} \perp \mathbf{x}$. The case $\boldsymbol{\tau} \perp Z$ represents orthoaxial projection. Points indicate an arbitrary distribution of projection directions $\boldsymbol{\tau}$.

2.5.6.2. 3D reconstruction in the general case

In the general case of the 3D reconstruction of $\varphi_3(\mathbf{r})$ from projections $\varphi_2(\mathbf{x}_\tau)$, the projection vector $\boldsymbol{\tau}$ occupies arbitrary positions on the projection sphere (Fig. 2.5.6.2). First, let us consider the case of a 2D function $\rho_2(\mathbf{x})$ and its ray transform $\varphi_1(x, \psi)$. We introduce an operation of backprojection b, which is stretching along $\boldsymbol{\tau}_\psi$ each 1D projection $\varphi_1(x_\psi)$ (Fig. 2.5.6.3). When the result is integrated over the full angular range of projections $\varphi_1(x, \psi)$, we obtain the projection synthesis defined as

$$b(x, y) = \int_0^\pi \varphi_1(x \cos\psi + y \sin\psi, \psi)\, \mathrm{d}\psi. \tag{2.5.6.9}$$

However, the backprojection operator is not the inverse of a 2D ray transform, as the resulting image b is blurred by the point-spread function $(x^2 + y^2)^{-1/2}$ (Vainshtein, 1971):

$$b(x, y) = \rho(x, y) * (x^2 + y^2)^{-1/2}. \tag{2.5.6.10}$$

By noting that the Fourier transform of $(x^2 + y^2)^{-1/2}$ is $(u^2 + v^2)^{-1/2}$ and by using the convolution theorem $\mathscr{F}[f * g] = \mathscr{F}[f]\mathscr{F}[g]$, we obtain the 'backprojection-filtering' inversion formula:

$$\begin{aligned}\rho(x, y) &= b(x, y) * (x^2 + y^2)^{1/2} = \mathscr{F}^{-1}\big[|\mathbf{u}|\mathscr{F}[b]\big] \\ &= \text{Filtration}_{|\mathbf{u}|}[\text{Backprojection}(\varphi_1)].\end{aligned} \tag{2.5.6.11}$$

The more commonly used 'filtered-backprojection' inversion is based on the 2D version of the central section theorem (2.5.6.8):

$$\mathscr{F}[\varphi_1(x_\psi)] = \Upsilon_2(\mathbf{u}_\psi) = \Upsilon_2(R, \Psi), \tag{2.5.6.12}$$

where $\mathscr{F}[\rho_2] = \Upsilon_2$. With this in mind, $\rho_2(\mathbf{x})$ can be related to its ray transform by evaluating the Fourier transform of ρ_2 in polar coordinates:

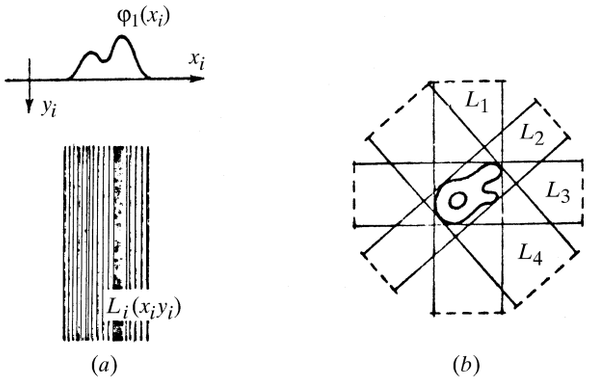

Fig. 2.5.6.3. (*a*) Formation of a backprojection function; (*b*) projection synthesis (2.5.6.9) is a superposition of these functions.

$$\begin{aligned}\rho_2(\mathbf{x}) &= \int \Upsilon_2(\mathbf{u}) \exp(-2\pi i \mathbf{u}\mathbf{x})\, \mathrm{d}\mathbf{u} \\ &= \int_0^{\pi} \int_{-\infty}^{\infty} \Upsilon_2(R, \Psi) \exp(-2\pi i \mathbf{x}\boldsymbol{\tau}) |R|\, \mathrm{d}R\, \mathrm{d}\Psi \\ &= \int_0^{\pi} \int_{-\infty}^{\infty} \mathscr{F}[\varphi_1(x_\psi)] \exp(-2\pi i \mathbf{x}\boldsymbol{\tau}) |R|\, \mathrm{d}R\, \mathrm{d}\Psi \\ &= \int_0^{\pi} \mathscr{F}^{-1}\big[|R| \mathscr{F}[\varphi_1(x_\psi)]\big]\, \mathrm{d}\Psi \\ &= \text{Backprojection}[\text{Filtration}_{|R|}(\varphi_1)]. \end{aligned} \quad (2.5.6.13)$$

In three dimensions, the backprojection stretches each 2D projection $\varphi_{2_i}[\mathbf{x}, \boldsymbol{\tau}(\theta, \psi)_i]$ along the projection direction $\boldsymbol{\tau}(\theta, \psi)_i$. A 3D synthesis is the integral over the hemisphere (Fig. 2.5.6.2)

$$b(\mathbf{r}) = \int_{\omega} \varphi_2(\mathbf{x}, \omega_{\boldsymbol{\tau}})\, \mathrm{d}\omega_{\boldsymbol{\tau}} = \varphi_3(\mathbf{r}) * (x^2 + y^2 + z^2)^{-1}. \quad (2.5.6.14)$$

Thus, in three dimensions the image b obtained using the backprojection operator is blurred by the point-spread function $1/(x^2 + y^2 + z^2)$ (Vainshtein, 1971). It is possible to derive inversion formulae analogous to (2.5.6.11) and (2.5.6.13).

The inversion formulae demonstrate that it is possible to invert the ray transform for continuous functions and for a uniform distribution of projections. In electron microscopy, the projections are never distributed uniformly in three dimensions. Indeed, a uniform distribution is not even desirable, as only certain subsets of projection directions are required for the successful inversion of a 3D ray transform, as follows from the central section theorem (2.5.6.8). In practice, we always deal with sampled data and with discrete, random and nonuniform distributions of projection directions. Therefore, the inversion formulae can be considered only as a starting point for the development of the numerical (and practical!) reconstruction algorithms. According to (2.5.6.10) and (2.5.6.14), a simple backprojection step results in reconstruction that corresponds to a convolution of the original function with a point-spread function that depends only on the distribution of projections, but not on the structure itself. Taking into account the linearity of the backprojection operation, one has to conclude that for any practically encountered distribution of projections it should be possible to derive the corresponding point-spread function and then, using either deconvolution or Fourier filtration (with a 'weighting function'), arrive at a good approximation of the structure. This observation forms the basis of the weighted backprojection algorithm (Section 2.5.6.5). Similarly, the central section theorem gives rise to direct Fourier inversion algorithms (Section 2.5.6.6). Nevertheless, since the data are discrete, the most straightforward methodology is to discretize and approach the reconstruction problem as an algebraic problem (Section 2.5.6.4).

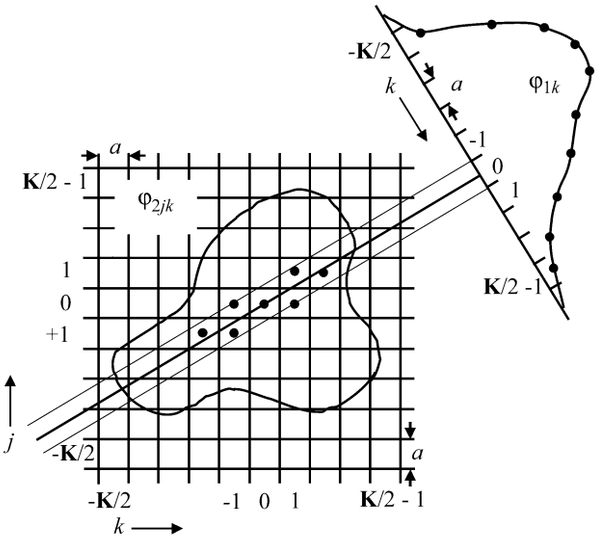

Fig. 2.5.6.4. Discretization in two dimensions ($d = 2$). The assumption is that the mass is located at the centre of the voxel.

2.5.6.3. Discretization and interpolation

In digital image processing, space is represented by a multidimensional discrete lattice. (It is sometimes expedient to use cylindrical or spherical coordinates, but these also have to be appropriately discretized.) The 2D projections $\varphi_2(\mathbf{x})$ are sampled on a Cartesian grid $\{\mathbf{k}a : \mathbf{k} \in \mathbf{Z}^d, (-\mathbf{K}/2) \leq \mathbf{k} \leq (\mathbf{K}/2)\}$, where d is the dimensionality of the grid ($d = 2$ for projections, $d = 3$ for the reconstructed object), $\mathbf{K} \in \mathbf{Z}_+^d$ is the size of the grid and a is the grid spacing (Fig. 2.5.6.4). In single-particle reconstruction, the units of a are usually ångstroms and we also assume that the data were appropriately sampled, *i.e.*, $a \leq (1/2u_{\max})$. Thus, the pixel size is less than or equal to the inverse of twice the maximum spatial frequency present in the data. Since the latter is not known in advance, a more practical rule is to select the pixel size at about one third of the expected resolution of the final structure, so that the adverse effects of interpolation are reduced.

The input electron microscopy data (projections of the macromolecule) are discretized on a 2D Cartesian grid, but each projection has a particular orientation in polar coordinates. Except for a few cases (projection directions parallel to the axes of the coordinate system of the 3D structure), an interpolation is required to relate measured samples to the voxel (volume pixel) values on the 3D Cartesian grid of the reconstructed structure (Fig. 2.5.6.4). The step of backprojection can be visualized as a set of rays with base a^{d-1} extended from projections and the ray values being added to the intersected voxels on the grid of the reconstructed structure (Figs. 2.5.6.3 and 2.5.6.4). One can select schemes that aim at approximation of the physical reality of the data collection, for example to weight the contributions by the areas of the voxels intersected by the ray or by the lengths of the lines that transverse the voxel (Huesman *et al.*, 1977). In order to reduce the time of calculations, in electron microscopy one usually assumes that all the mass is located at the centre of the voxel and the additional accuracy is achieved by application of tri- (or bi-)linear interpolation. The exception is the algebraic reconstruction technique with blobs algorithm (Marabini *et al.*, 1998), where the voxels are represented by smooth spherically symmetric volume elements [for example, the Keiser–Bessel function (2.5.6.44)].

In real space, both the projection and backprojection steps can be implemented in two different ways: as voxel driven or as ray driven (Laurette *et al.*, 2000). If we consider a projection, in the